International Journal of Pharmaceutics 410 (2011) 118–124

Contents lists available at ScienceDirect

International Journal of Pharmaceutics

journal homepage: www.elsevier.com/locate/ijpharm

Pharmaceutical Nanotechnology

Inclusion of the poorly water-soluble drug simvastatin in mesocellular foam nanoparticles: Drug loading and release properties

Yanzhuo Zhang[a], Jinghai Zhang[b], Tongying Jiang[a], Siling Wang[a,*]

[a] Department of Pharmaceutics, School of Pharmacy, Shenyang Pharmaceutical University, Shenyang 110016, PR China
[b] Key Laboratory of Pharmaceutical Biotechnology, School of Life Science and Bio-pharmaceutics, Shenyang Pharmaceutical University, Shenyang 110016, PR China

ARTICLE INFO

Article history:
Received 18 May 2010
Received in revised form 21 July 2010
Accepted 21 July 2010
Available online 30 July 2010

Keywords:
Drug delivery
Mesocellular foam
Poorly water-soluble drugs
Simvastatin
Drug loading
Enhanced dissolution

ABSTRACT

The purpose of this study was to develop spherical mesocellular foam (MCF) loaded with a poorly water-soluble drug, intended to be orally administered, able to improve the dissolution rate and enhance the drug loading capacity. Spherical MCF with a continuous 3-D pore system was synthesized using Pluronic 123 triblock polymer (P123) as a surfactant coupled with cetyltrimethyl ammonium bromide (CTAB) as a co-surfactant. A model drug, simvastatin (SV), was loaded onto spherical MCF via a procedure involving a combination of adsorption equilibrium and solvent evaporation. The drug release rate and the drug loading efficiency of spherical MCF were compared with those of fibrous SBA-15. Investigations using nitrogen adsorption, scanning electron microscopy (SEM), transmission electron microscopy (TEM), powder X-ray diffraction (PXRD), differential scanning calorimetry (DSC), thermogravimetric analysis (TGA) and HPLC demonstrated the successful incorporation of SV into the MCF host. It was found that spherical MCF has a high drug loading efficiency up to 37.5%, and higher than that of fibrous SBA-15 with a pore diameter of 6.5 nm. It is worth noting that fast release rate of SV was obtained from spherical MCF compared with SBA-15 and pure crystalline SV using enzyme-free simulated intestinal fluid (SIF, pH 6.8).

1. Introduction

The oral delivery route is commonly recognized as the most preferred and convenient route for the administration of drug formulations. In order for a drug to be absorbed into the systemic circulation following oral administration, it must be dissolved in gastrointestinal (GI) fluids. For hydrophobic drugs belonging to Class II of the Biopharmaceutical Classification System (BCS), it is this dissolution process which acts as the rate-controlling step and, therefore, determines the rate and degree of absorption (Lipinski, 2002; Vasconcelos et al., 2007). Consequently, many hydrophobic drugs show incomplete absorption from the GI tract. Thus, one of the major current challenges facing the pharmaceutical industry involves the development of strategies to improve the water solubility and dissolution rate of drugs, since it is estimated that 40% of new chemical entities (NCE) are poorly soluble or insoluble in water (Lipinski et al., 2001; Gursoy and Benita, 2004; Wong et al., 2006; Kesisoglou et al., 2007; Sachs-Barrable et al., 2008).

In the past decade, mesoporous silica has found widespread application as controlled drug delivery systems (DDS) (Fu et al., 2003; Mal et al., 2003; Barbé et al., 2004; Charnay et al., 2004; Chen et al., 2004; Slowing et al., 2007; Wu et al., 2007; Wang, 2009). Mesoporous silica offer several attractive features for controlled release, such as a high adsorption capacity (Kresge et al., 1992; Zhao et al., 1998; Mal et al., 2003; Lin et al., 2005; He et al., 2010); the homogeneity of the drug distribution in the host is achieved by the well-ordered pore arrangement (Cauda et al., 2009; Thomas et al., 2009) and it is easy to modify the pore dimensions to control the drug delivery kinetics (Yang et al., 2008; Wang, 2009). In addition to the pore channels of mesoporous materials being able to change the crystalline state of a drug to an amorphous one, the pore channels also restrict drug recrystallization and reduce the particle size of the amorphous drug (Charnay et al., 2004; Salonen et al., 2005; Ambrogi et al., 2007; Thomas et al., 2009). So far, the most often used mesoporous silica-based drug carriers have been the MCM series and the SBA series. Typically, the pore diameter varies between 2 and 6 nm for MCM-41 and between 4 and 13 nm for SBA-15 (Mellaerts et al., 2008; Wang, 2009). However, the focus of mesoporous silica has been mainly the development of slow release formulations, and fewer reports have been published on the application of synthetic mesoporous silica involving the dissolution enhancement of poorly water-soluble drugs (Song et al., 2005; Qu et al., 2006; Mellaerts et al., 2008; Li et al., 2009; Wang, 2009; Yu and Zhai, 2009). The main reasons for slow release involve the pore size and geometry of the pore network (Heikkilä et al., 2007; Yang et al., 2008). The pore size is an important factor affecting the drug release rate

* Corresponding author at: Shenyang Pharmaceutical University P.O. Box 32, 103 Wenhua Road, Shenhe District, Shenyang, Liaoning Province 110016, PR China. Tel.: +86 24 23986348; fax: +86 24 23986348.
E-mail address: silingwang310@sina.com (S. Wang).

0378-5173/$ – see front matter © 2010 Elsevier B.V. All rights reserved.
doi:10.1016/j.ijpharm.2010.07.040

and it has been found that reducing the pore size can delay the release of a drug (Horcajada et al., 2004; Qu et al., 2006; Yang et al., 2008). In addition, the majority of mesoporous silica materials exhibit sterical diffusion hindrance caused by the 2-D hexagonally ordered long pore channels as far as drug loading and diffusion is concerned. For example, the length of unidirectional pore channels varies between 1 and 20 μm for SBA-15 (Qu et al., 2006; Heikkilä et al., 2007; Li et al., 2009). To overcome these problems it is essential to develop a novel drug-loaded mesoporous silica material in a way that allows an enhanced dissolution rate. Mesocellular foam (MCF) is composed of uniformly sized, large spherical cells that are interconnected by uniform windows to create a continuous 3-D pore system (Schmidt-Winkel et al., 1999; Lettow et al., 2000). The interconnected nature of the large uniform pores makes this mesostructured silica a promising candidate for a drug delivery device with fast release properties (Heikkilä et al., 2007).

The purpose of this study was to develop spherical MCF loaded with a poorly water-soluble drug, intended to be orally administered, able to improve the dissolution rate and enhance the drug loading capacity. SV, a well-known cholesterol-lowering drug, was selected as a model drug due to its very poor aqueous solubility (solubility at 25 °C, 6.3 μg/ml, pH 1–7) as a BCS class II drug (Ambike et al., 2005; Graeser et al., 2008; Zhang et al., 2009). The effects of the large pore size and 3-D pore system of MCF on the uptake and release of the model drug SV were systematically studied using nitrogen adsorption, scanning electron microscopy (SEM), transmission electron microscopy (TEM), powder X-ray diffraction (PXRD), differential scanning calorimetry (DSC), thermogravimetric analysis (TGA) and HPLC.

2. Materials and methods

2.1. Materials

Guaranteed-grade tetraethyl orthosilicate (TEOS), cetyltrimethyl ammonium bromide (CTAB), 1,3,5-trimethylbenzene (TMB), ammonia tetrafluoride, HPLC-grade methanol, acetonitrile, phosphoric acid, sodium dihydrogen phosphate, hydrochloric acid and sodium hydroxide were purchased from Aladdin (Shanghai, China). Pluronic 123 triblock polymer (P123) [$(EO)_{20}(PO)_{70}(EO)_{20}$, molecular weight, MW = 5800] was purchased from Sigma–Aldrich (St. Louis, MO, USA). Simvastatin (SV, ≥98%) was kindly donated by Hisun (Zhejiang, China). Deionized water was prepared by a Milli-Q purification system obtained from Millipore (Bedford, MA, USA). All other chemicals were of reagent grade and were used as purchased without further purification.

2.2. Synthesis of spherical MCF nanoparticles

Spherical MCF nanoparticles were synthesized in aqueous hydrochloric acid using P123 as a structure-directing agent and TMB as a micelle expander. In a typical synthesis, 2.4 g P123 was dissolved in 90 ml 1.6 M hydrochloric acid solution at room temperature. Then, 0.4 g CTAB, 0.025 g ammonia tetrafluoride and 1.6 ml TMB were added to the surfactant solution, the mixture was stirred for 2 h, and 5.5 ml TEOS was added dropwise to the surfactant solution under vigorous stirring. The stirring was allowed to continue for another 5 min before switching to static synthesis conditions at 38 °C. After 20 h, the milky reaction mixture was transferred to a Teflon-lined autoclave and crystallized for another 24 h at 120 °C. As-synthesized material was filtered, washed with ethanol, and dried at 60 °C in a vacuum oven. Finally, the resulting powder was calcined in air at 600 °C for 5 h at a heating rate of 2 °C/min to remove the organic template.

Fibrous SBA-15 microparticles were synthesized by the procedure reported by Zhao et al. (1998) with some modifications. Briefly, 2.0 g P123 was dissolved in a mixture of 15 ml water and 60 ml 2 M hydrochloric acid solution with constant stirring at 38 °C then, after 1 h, 4.6 ml TEOS was added to this solution. Following this, the reaction solution was stirred for 24 h at 38 °C and the mixed solution was then crystallized at 90 °C for 24 h. The solid product was filtered, washed with ethanol, dried in air, and calcined at 600 °C for 5 h.

2.3. SV loading procedure

SV adsorption to MCF was carried out by soaking the MCF nanoparticles in an ethanol solution of SV (100 mg/ml). Ethanol was used as the loading solvent because it is safe, nontoxic, and can dissolve large amounts of SV. The carrier:drug ratio in the loading solution ranged from 5:1 to 1:1 (w:w). Then, the mixture was ultrasonicated for a few minutes and brought to adsorption equilibrium under gentle vortexing for 12 h in order to achieve maximum loading in the pore channels of the MCF nanoparticles. The loading was performed under ambient conditions (about 20 °C) in closed containers to prevent evaporation of ethanol during the loading period. Finally, the mixture was dried at 55 °C under vacuum for over a day. The drug-loaded sample was referred to as SV–MCF. The procedure for SV loading into the SBA-15 microparticles was similar to that used for loading MCF. The dried drug-loaded sample was referred to as SV–SBA-15.

2.4. SEM and TEM studies

The morphology and particle size of the prepared samples were characterized using a JSM-6301F SEM instrument (JEOL, Japan) operated at 15 kV. The samples were gold-plated prior to imaging. The porous structure of the samples was characterized using a Tecnai G^2 F30 TEM instrument (FEI, The Netherlands) operated at 200 kV. Before examination, the samples were dispersed in deionized water through sonication and subsequently deposited on carbon-coated copper grids.

2.5. Nitrogen adsorption analysis

The pore characteristics of the samples were studied by determining the nitrogen adsorption using a SA3100 surface area and pore size analyzer (Beckman Coulter, USA) at −196 °C. The specific surface area, S_{BET}, was evaluated from nitrogen adsorption data over the relative pressure range from 0.05 to 0.2 using the Brunauer–Emmett–Teller (BET) method. The total pore volume, V_t, was determined from the amount adsorbed at a relative pressure of 0.99. Pore size distributions (PSDs) were determined from adsorption branches of isotherms using the Barrett–Joyner–Halenda (BJH) method with the Kelvin equation for a hemispherical meniscus and the statistical film thickness curve for macroporous silica. The BJH pore diameter, w_{BJH}, is defined as the maximum on the pore size distribution curve. The MCF (or SBA-15) samples were degassed at 300 °C for 12 h prior to analysis, while the SV-loaded samples were degassed at 50 °C for 12 h. The experiments were performed in triplicate.

2.6. PXRD and DSC studies

PXRD was used for the identification of the crystals (structure and changes) of the SV-loaded samples and also the pure crystalline SV. PXRD patterns of the prepared samples were obtained using an X'pert PRO diffractometer (PANalytical B.V., The Netherlands), with an Ni filtered Cu-Ka line as the source of radiation, and the equipment was operated at a voltage of 40 kV and a current of 30 mA.

All samples were measured over the 2θ angle range from 5° to 40° with a scan rate of 4°/min and a step size of 0.02°. The physical state of the pure crystalline SV and the SV-loaded samples was also examined by DSC. The thermographs of each powder were obtained using a DSC 1 Star^e instrument (Mettler Toledo, Switzerland). The SV-loaded samples equivalent to 4 mg SV and pure crystalline SV (4 mg) were placed in pierced aluminum pans and heated from 50 to 200 °C at a scanning rate of 10 °C/min under a nitrogen purge of 40 ml/min.

2.7. HPLC analysis and TGA

SV was analyzed using a Hitachi^{TM} HPLC system consisting of an L2100 pump, an L2200 autosampler, a LaChrom Elite Smash system controller, an L2300 column oven and an L2420 UV–VIS tunable absorbance detector set at 238 nm (Japan). Analysis was carried out on a Shim-pack C_{18} column (250 × 4.6 mm, 5 μm). The mobile phase consisted of acetonitrile and 25 mM sodium dihydrogen phosphate solution (adjusted to pH 4.5 with phosphoric acid) in a volume ratio of 75/25 (v/v) which was eluted at a flow rate of 1.0 ml/min. The injection volume was 10 μl. The sample was passed through a 0.22 μm polytetrafluoroethylene (PTFE) membrane filter before the HPLC analysis.

The drug loading was determined by extracting 10 mg of the SV-loaded samples with 200 ml methanol for 12 h with stirring, followed by filtration of the sample and analysis by HPLC (Salonen et al., 2005; Thomas et al., 2009). The drug loading was also quantified by TGA (Salonen et al., 2005; Heikkilä et al., 2007; Kapoor et al., 2009). TGA was performed with a TGA-50 instrument (Shimadzu, Japan) with a heating rate of 10 °C/min under a nitrogen purge of 40 ml/min. The experiments were performed in triplicate. The drug loading was calculated using the following equation (1):

$$\text{Drug loading}(\%) = \frac{\text{weight of drug in nanoparticles}}{\text{weight of nanoparticles}} \times 100 \quad (1)$$

2.8. Solubility study

The solubility of SV was determined in triplicate in phosphate buffer solution (pH 6.8) by adding an excess amount of pure crystalline SV and SV-loaded samples (ca. 10 mg as SV) to different snap-cap Eppendorf tubes. The resulting mixtures were vortexed and then placed in a constant temperature shaking bath maintained at 37 ± 0.5 °C until equilibrium was reached (for 48 h). Suitable aliquots were centrifuged at 12,000 rpm for 15 min. The supernatant layer was removed, suitably diluted and then the drug concentration was determined by HPLC (Ambike et al., 2005; Zhang et al., 2009).

2.9. In vitro drug release study

The *in vitro* drug release study was conducted using a USP II dissolution tester (RCZ-8A, Tianjin University Radio Factory, China). The SV-loaded samples equivalent to 10 mg SV were placed in the dissolution vessels containing 900 ml enzyme-free simulated intestinal fluid (SIF) (pH 6.8), maintained at 37 ± 0.1 °C and stirred at 100 rpm (Ambike et al., 2005). Enzyme-free SIF (pH 6.8) prepared by adding 6.8 g potassium dihydrogen phosphate in deionized water and adjusting the pH with 0.1 M sodium hydroxide solution to obtain 1 L enzyme-free SIF. At predetermined time intervals, 5 ml samples were withdrawn and immediately replaced with an equal volume of dissolution medium to keep the volume constant. The withdrawn samples were filtered and the concentration of SV was then analysis by HPLC. All data were reported as the mean ± standard deviation (SD). Statistical analysis was performed for the experiments conducted in triplicate using Student's *t*-test. Results with $p < 0.05$ were considered to be statistically significant.

3. Results and discussion

3.1. Morphology and particle size of the prepared nanoparticles

SEM imaging showed that the prepared MCF sample consisted of many spherical particles with a relatively uniform size of about 800 nm in diameter (Fig. 1a). The TEM micrograph of MCF nanoparticles also revealed that these were spherical, with dimensions similar to those found by SEM measurements (Fig. 1b). Examination of these nanoparticles at higher magnifications showed that they had a porous structure (Fig. 1c). MCF was composed of uniformly sized, large spherical cells that were interconnected by uniform windows to create a continuous 3-D pore system. In addition, the TEM image of SV–MCF clearly showed that the 3-D pore structures were still present in the SV-loaded samples (Fig. 1d).

SEM imaging showed that the SBA-15 sample consisted of many rod-like sub-particles of relatively uniform size of about 0.4 μm in diameter and 1–2 μm in length, which had aggregated into wheat-like macrostructures (Fig. 2a). Similar SEM images have been reported by Katiyar et al. (2006). As shown in Fig. 2b, the TEM micrograph of SBA-15 was recorded with the electron beam direction nearly parallel to the channel direction. The TEM image confirmed the ordered structure of SBA-15, and showed that the cylindrical pores were arranged in an ordered fashion. In addition to the different pore geometries, the pore size of MCF was approximately 4-fold larger than that of SBA-15.

3.2. Nitrogen adsorption analysis

The nitrogen adsorption/desorption isotherms of the prepared MCF samples were typical type IV isotherms according to the IUPAC classification, characteristic of mesoporous materials (Zhao et al., 1998; Lettow et al., 2000). As an example, the nitrogen adsorption/desorption isotherms of MCF and SV–MCF are presented in Fig. 3, and the nitrogen adsorption/desorption isotherms of SBA-15 and SV–SBA-15 are presented in Fig. 4. The isotherms of MCF (or SBA-15) featured hysteresis loops with sharp adsorption and desorption branches. The values for the BET specific surface area (S_{BET}), the total pore volume (V_t) and the BJH pore diameter (w_{BJH}) are given in Table 1. It can be seen that the MCF (or SBA-15) samples have a high S_{BET} and V_t, indicating its potential application as a host for bonding or storing more drug molecules in the drug storage/release system. Furthermore, S_{BET}, V_t and w_{BJH} were reduced apparently after SV had been loaded, confirming that SV was incorporated into MCF (or SBA-15) pore channels (Chen et al., 2004; Yang et al., 2008; Kapoor et al., 2009).

3.3. Physicochemical characterization

The PXRD patterns of the drug-loaded samples were recorded to determine whether a crystalline drug phase would be detected (Charnay et al., 2004; Heikkilä et al., 2007; Kapoor et al., 2009; Yu and Zhai, 2009). The PXRD patterns of SV, MCF, physical mixture and SV–MCF are given in Fig. 5. The diffraction pattern of pure SV was highly crystalline in nature as indicated by numerous peaks. The main peaks at 9.3°, 15.6°, 16.5°, 17.2°, 17.7°, 18.8°, 19.4° and 22.5° were particularly distinctive. For the physical mixture of SV and MCF, numerous peaks were attributed to pure SV. However, no crystalline SV was detected in the SV–MCF_1 samples (Fig. 5e, the mass ratio of MCF:SV was 5:3 in the drug loading procedure). In contrast, SV peaks at 9.3°, 16.5°, 17.2° and 22.5° were observed in the SV–MCF_2 samples (Fig. 5d, the mass ratio of MCF:SV was 5:4 in the drug loading procedure). It was found that the prepared MCF nanoparticles had a high drug loading efficiency up to 37.5% (Fig. 6c). On the other hand, no crystalline SV was detected in the SV–$SBA\text{-}15_1$ samples (the mass ratio of SBA-15:SV was 5:2 in the

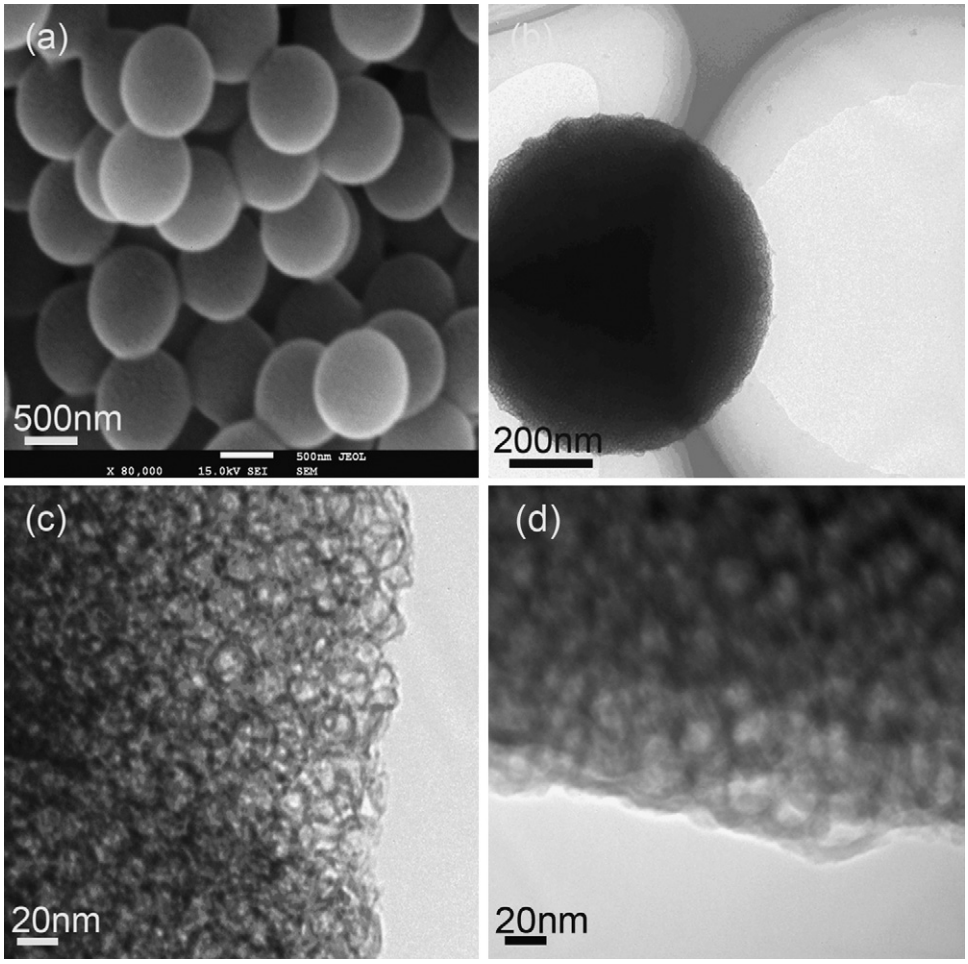

Fig. 1. SEM photograph of (a) MCF; TEM photographs of (b) MCF, (c) MCF (enlarged) and (d) SV–MCF.

drug loading procedure). In contrast, SV peaks were observed in the TEL-SBA-15_2 samples (the mass ratio of SBA-15:SV was 5:3 in the drug loading procedure). It was found that the maximum drug loading efficiency of the prepared SBA-15 microparticles was approximately 28.6% (Fig. 6b). The drug loading values obtained by HPLC were in agreement with those obtained by TGA, as shown in Table 1. In agreement with previous reports, the drug loading capacity of mesoporous material was very dependent on its S_{BET} and V_t. The relatively high S_{BET} and V_t of mesoporous material enable it to achieve a high drug loading efficiency (Yang et al., 2008; Thomas et al., 2009). However, there were some differences in the maximum drug loading efficiency of the prepared particles, the MCF samples (V_t was 1.73 cm^3/g) exhibited a higher drug loading efficiency than the SBA-15 samples (V_t was 1.21 cm^3/g), while the S_{BET} of MCF was less than that of SBA-15.

The presence or absence of crystalline drug was also confirmed by DSC analysis using the drug melting peak in the thermograms as an indication that SV was in crystalline form in the sample. When in its crystalline form in the pores, the amount of drug can be estimated from the melting point depression using DSC. If the drug in the pores is in a noncrystalline state, no melting point depression can be detected (Salonen et al., 2005; Mellaerts et al., 2008; Thomas et al., 2009; Wang, 2009). Thermograms of SV–MCF were recorded and signals due to melting could be observed. As an example, the DSC curves for SV, MCF and SV–MCF are presented in Fig. 7. DSC analysis of crystalline SV showed a single sharp endothermic peak at 138.6 °C, which corresponded to its intrinsic melting point (the endothermic value was 79.51 ± 0.07 J/g). No characteristic melting peak of SV was identified in the DSC curve obtained from SV–MCF_1 (Fig. 7c). The absence of phase transitions owing to SV in the DSC analysis is evidence that SV is in an amorphous state. In contrast, the melting peak of SV was observed at 181.3 °C in the DSC curve obtained from SV–MCF_2 (Fig. 7b, the endothermic value was 3.42 ± 1.29 J/g), which confirms the results obtained from the PXRD study.

3.4. Solubility study

The solubility testing showed increased solubility for an amorphous state of SV compared to the crystalline state. The solubility

Table 1
Results of sample characterizations ($n = 3$).

Sample	S_{BET} (m^2/g)	V_t (cm^3/g)	w_{BJH} (nm)	Drug loading HPLC (%)	Drug loading TGA (%)
MCF	816.0 ± 7.2	1.73 ± 0.04	28.3 ± 2.4	–	–
SV–MCF	232.5 ± 21.7	0.82 ± 0.15	22.5 ± 3.3	36.9 ± 1.2	37.5 ± 0.8
SBA-15	982.4 ± 5.6	1.21 ± 0.03	6.5 ± 1.7	–	–
SV–SBA-15	259.7 ± 30.2	0.51 ± 0.12	3.1 ± 1.4	27.4 ± 2.3	28.6 ± 1.5

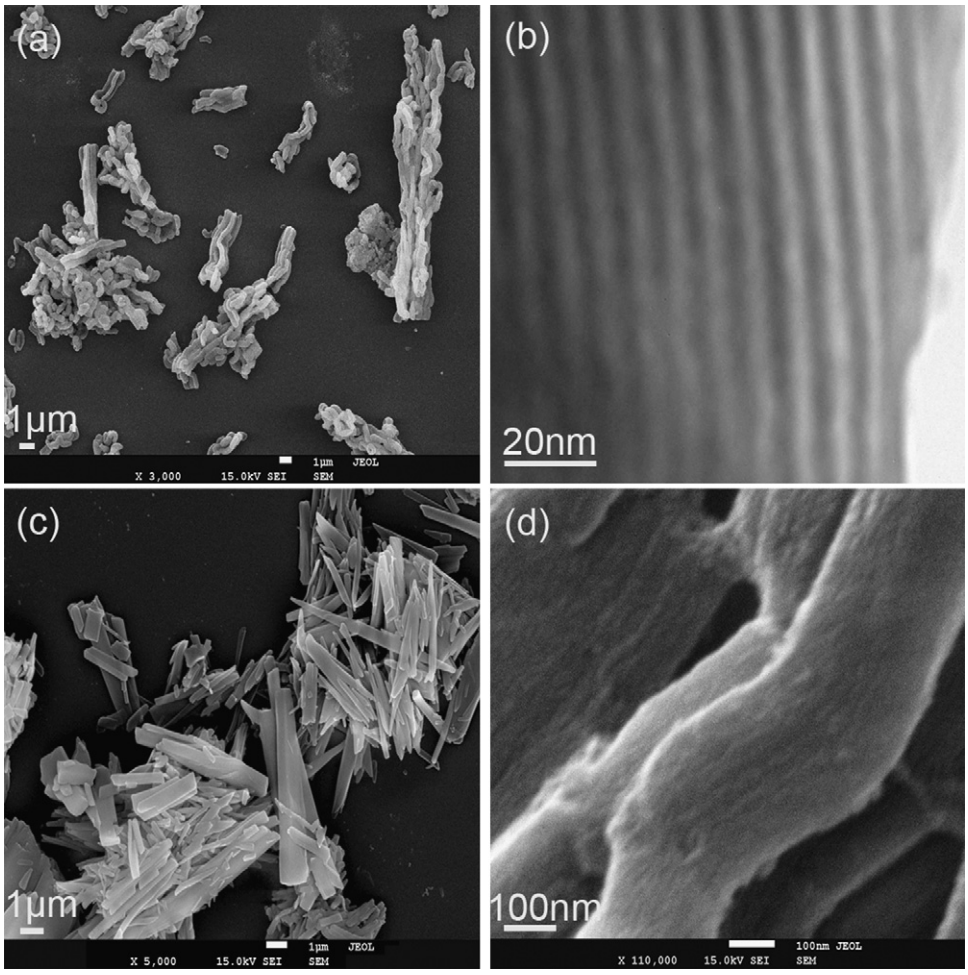

Fig. 2. SEM photographs of (a) SBA-15, (c) pure SV and (d) SV–SBA-15; TEM photograph of (b) SBA-15.

of crystalline SV was 15.7 ± 0.4 μg/ml, which agreed with the literature (Zhang et al., 2009). SV incorporation into MCF or SBA-15 resulted in an approximately 4-fold increase in solubility after 48 h (60.5 ± 2.1 μg/ml for MCF and 55.2 ± 3.9 μg/ml for SBA-15) in comparison with crystalline SV.

3.5. In vitro drug release study

The effects of different pore sizes and pore structures on the SV release rate in enzyme-free SIF (pH 6.8) is shown in Fig. 8. Crystalline SV and SV–SBA-15 exhibited poor dissolution rates in

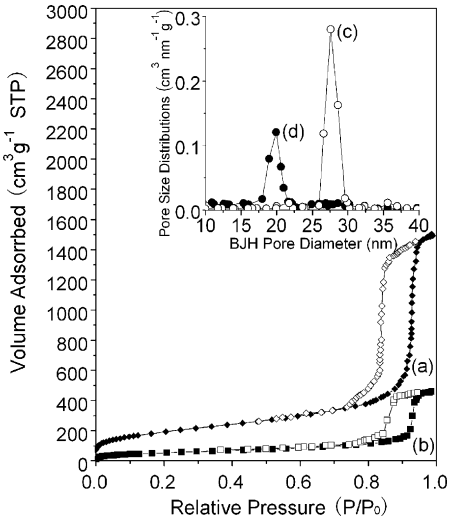

Fig. 3. Nitrogen adsorption/desorption isotherms of (a) MCF and (b) SV–MCF. Pore size distributions of (c) MCF and (d) SV–MCF.

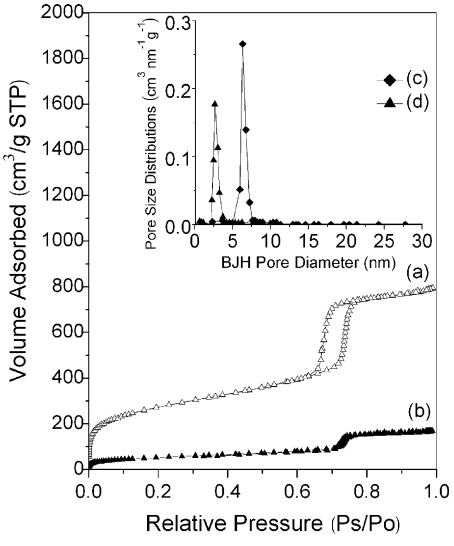

Fig. 4. Nitrogen adsorption/desorption isotherms of (a) SBA-15 and (b) SV–SBA-15. Pore size distributions of (c) SBA-15 and (d) SV–SBA-15.

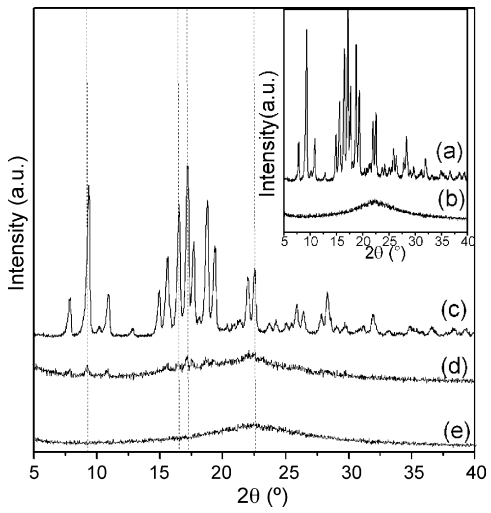

Fig. 5. PXRD patterns of (a) SV, (b) MCF, (c) physical mixture, (d) SV–MCF_2 and (e) SV–MCF_1.

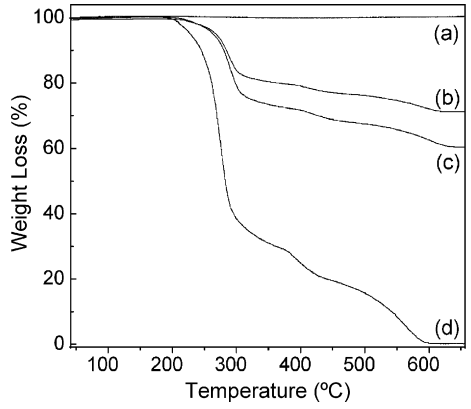

Fig. 6. TGA of (a) MCF, (b) SV–SBA-15, (c) SV–MCF and (d) SV.

enzyme-free SIF, and the amounts of dissolved SV from the pure crystalline SV and SV–SBA-15 at sampling time of 60 min was found to be ca. 17% and 62%, respectively. In contrast, SV–MCF showed the accelerated dissolution behavior as evidenced by release of ca. 89% SV from SV–MCF at 20 min. The dissolution improvement may be largely attributed to the pore channels of the two carriers changing the crystalline state of SV to an amorphous state, which is known to improve the drug solubility and dissolution rate (Salonen et al., 2005; Heikkilä et al., 2007; Vasconcelos et al., 2007). In addition, the particle sizes of the amorphous drug incorporated in the pore

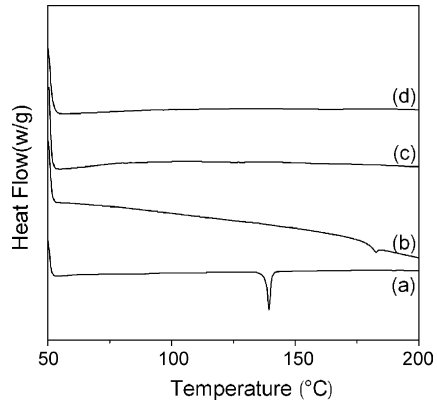

Fig. 7. DSC thermograms of (a) SV, (b) SV–MCF_2, (c) SV–MCF_1 and (d) MCF_2.

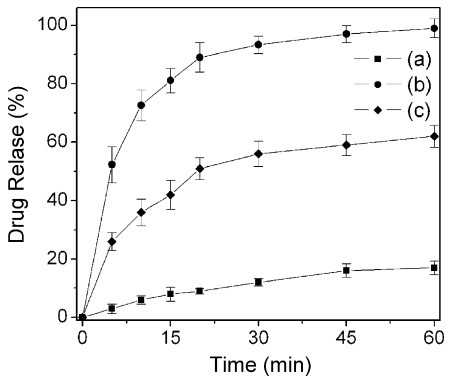

Fig. 8. Dissolution profiles of SV from (a) pure crystalline SV, (b) SV–MCF and (c) SV–SBA-15 in enzyme-free SIF (pH 6.8). Each data point represents the mean ± SD of three determinations.

channels (nanometer range) were significantly reduced compared with that of pure crystalline SV (micron range). It is evident that a further decrease in the particle size down to the nanometer range will further accelerate the drug release profile and, consequently, improve the dissolution rate (Salonen et al., 2005; Kesisoglou et al., 2007; Vasconcelos et al., 2007). It is obviously shown that the faster SV release of the two drug-loaded samples was observed from SV–MCF. The difference in release rate between MCF and SBA-15 could be attributed to the pore sizes and pore structures. It is known that fast drug release can be achieved by enlarging the pore size of the mesoporous carrier (Horcajada et al., 2004; Qu et al., 2006; Mellaerts et al., 2008; Yang et al., 2008). Therefore, MCF (w_{BJH} was 28.3 nm) exhibited a lower steric diffusion hindrance caused by pore channels compared with SBA-15 (w_{BJH} was 6.5 nm). In addition, the SV molecules adsorbed in the 3-D spherical pore systems (spherical cells with relatively uniform sizes of about 25 nm in diameter, as shown in Fig. 1c) had a greater chance of escaping from mesopore channels and diffusing into the release medium compared with those adsorbed in the ordered 2-D cylindrical pore systems (pore channels with a relatively uniform size of about 6 nm in diameter and 1–2 μm in length, as shown in Fig. 2a and b).

4. Conclusions

The results of this study demonstrated the successful uptake and then release of a model drug in spherical MCF nanoparticles, confirming the potential of spherical MCF nanoparticles as a drug delivery system. MCF with a continuous 3-D pore system has a high drug loading efficiency up to 37.5%. The *in vitro* drug release study showed that the dissolution rate of SV released from MCF was significantly faster compared with crystalline SV. The dissolution improvement was associated with MCF converting the loaded drug from the solid state to the amorphous form, which typically dissolves faster compared with the crystalline form. In addition, our study shows that the differences in pore size and structure of mesoporous silica play an important role in controlling the release rate of drug molecules, with a faster release of SV from MCF compared with SBA-15. Since drug release is a crucial and limiting step for oral drug absorption, particularly for drugs with low GI solubility and high permeability, spherical MCF nanoparticles might offer a larger window of absorption for the drug in the GI tract by improving the dissolution rate of poorly water-soluble drugs.

Acknowledgements

This work was supported by the National Basic Research Program of China (973 Program) (No. 2009CB930300). We would like to thank Dr. David Jack for correcting language.

References

Ambike, A.A., Mahadik, K.R., Paradkar, A., 2005. Spray-dried amorphous solid dispersions of simvastatin, a low Tg drug: in vitro and in vivo evaluations. Pharm. Res. 22, 990–998.

Ambrogi, V., Perioli, L., Marmottini, F., Giovagnoli, S., Esposito, M., Rossi, C., 2007. Improvement of dissolution rate of piroxicam by inclusion into MCM-41 mesoporous silicate. Eur. J. Pharm. Sci. 32, 216–222.

Barbé, C., Bartlett, J., Kong, L., Finnie, K., Lin, H.Q., Larkin, M., 2004. Silica particles: a novel drug-delivery system. Adv. Mater. 16, 1949–1966.

Cauda, V., Muhlstein, L., Onida, B., Bein, T., 2009. Tuning drug uptake and release rates through different morphologies and pore diameters of confined mesoporous silica. Microporous Mesoporous Mater. 118, 435–443.

Charnay, C., Bégu, S., Tourné-Péteilh, C., Nicole, L., Lerner, D.A., Devoisselle, J.M., 2004. Inclusion of ibuprofen in mesoporous templated silica: drug loading and release property. Eur. J. Pharm. Biopharm. 57, 533–540.

Chen, J.F., Ding, H.M., Wang, J.X., Shao, L., 2004. Preparation and characterization of porous hollow silica nanoparticles for drug delivery application. Biomaterials 25, 723–727.

Fu, Q., Rama Rao, G.V., Ista, L.K., Wu, Y., Andrzejewski, B.P., Sklar, L.A., 2003. Control of molecular transport through stimuli-responsive ordered mesoporous materials. Adv. Mater. 15, 1262–1266.

Graeser, K.A., Strachan, C.J., Patterson, J.E., Gordon, K.C., Rades, T., 2008. Physicochemical properties and stability of two differently prepared amorphous forms of simvastatin. Cryst. Growth Des. 8, 128–135.

Gursoy, R.N., Benita, S., 2004. Self-emulsifying drug delivery systems (SEDDS) for improved oral delivery of lipophilic drug. Biomed. Pharmacother. 58, 173–182.

He, Q.J., Zhang, J.M., Shi, J.L., Zhu, Z.Y., Zhang, L.X., Bu, W.B., Guo, L.M., Chen, Y., 2010. The effect of PEGylation of mesoporous silica nanoparticles on nonspecific binding of serum proteins and cellular responses. Biomaterials 31, 1085–1092.

Heikkilä, T., Salonen, J., Tuura, J., Hamdy, M.S., Mul, G., Kumar, N., Salmi, T., Murzin, D.Y., Laitinen, L., Kaukonen, A.M., Hirvonen, J., Lehto, V.P., 2007. Mesoporous silica material TUD-1 as a drug delivery system. Int. J. Pharm. 331, 133–138.

Horcajada, P., Rámila, A., Pérez-Pariente, J., Vallet-Regi, M., 2004. Influence of pore size of MCM-41 matrices on drug delivery rate. Microporous Mesoporous Mater. 68, 105–109.

Kapoor, S., Hegde, R., Bhattacharyya, A.J., 2009. Influence of surface chemistry of mesoporous alumina with wide pore distribution on controlled drug release. J. Control. Release 140, 34–39.

Katiyar, A., Yadav, S., Smirniotis, P.G., Pinto, N.G., 2006. Synthesis of ordered large pore SBA-15 spherical particles for adsorption of biomolecules. J. Chromatogr. A 1122, 13–20.

Kesisoglou, F., Panmai, S., Wu, Y., 2007. Nanosizing – oral formulation development and biopharmaceutical evaluation. Adv. Drug Deliv. Rev. 59, 631–644.

Kresge, C.T., Leonowicz, M.E., Roth, W.J., Vartuli, J.C., Beck, J.S., 1992. Ordered mesoporous molecular sieves synthesized by a liquid-crystal template mechanism. Nature 359, 710–712.

Lettow, J.S., Han, Y.J., Schmidt-Winkel, P., Yang, P., Zhao, D., Stucky, G.D., Ying, J.Y., 2000. Hexagonal to mesocellular foam phase transition in polymer-templated mesoporous silicas. Langmuir 16, 8291–8295.

Li, Y.J., Zhou, G.W., Li, C.J., Qin, D.W., Qiao, W.T., Chu, B., 2009. Adsorption and catalytic activity of *Porcine pancreatic* lipase on rod-like SBA-15 mesoporous material. Colloids Surf. A 341, 79–85.

Lin, Y.S., Tsai, C.P., Huang, H.Y., Kuo, C.T., Hung, Y., Huang, D.M., Chen, Y.C., Mou, C.Y., 2005. Well-ordered mesoporous silica nanoparticles as cell markers. Chem. Mater. 17, 4570–4573.

Lipinski, C.A., 2002. Poor aqueous solubility – an industry wide problem in drug discovery. Am. Pharm. Rev. 53, 82–85.

Lipinski, C.A., Lombardo, F., Dominy, B.W., Feeney, P.J., 2001. Experimental and computational approaches to estimate solubility and permeability in drug discovery and development setting. Adv. Drug Deliv. Rev. 46, 3–26.

Mal, N.K., Fujiwara, M., Tanaka, Y., 2003. Photocontrolled reversible release of guest molecules from coumarin-modified mesoporous silica. Nature 421, 350–353.

Mellaerts, R., Mols, R., Jammaer, J.A.G., Aerts, C.A., Annaert, P., Humbeeck, J.V., Mooter, G.V., Augustijns, P., Martens, J.A., 2008. Increasing the oral bioavailability of the poorly water soluble drug itraconazole with ordered mesoporous silica. Eur. J. Pharm. Biopharm. 69, 223–230.

Qu, F.Y., Zhu, G.S., Huang, S.Y., Li, S.G., Sun, J.Y., Zhang, D.L., Qiu, S.L., 2006. Controlled release of captopril by regulating the pore size and morphology of ordered mesoporous silica. Microporous Mesoporous Mater. 92, 1–9.

Sachs-Barrable, K., Lee, S.D., Wasan, E.K., Thornton, S.J., Wasan, K.M., 2008. Enhancing drug absorption using lipids: a case study presenting the development and pharmacological evaluation of a novel lipid-based oral amphotericin B formulation for the treatment of systemic fungal infections. Adv. Drug Deliv. Rev. 60, 692–701.

Salonen, J., Laitinen, L., Kaukonen, A.M., Tuura, J., Björkqvist, M., Heikkilä, T., Vähä-Heikkilä, K., Hirvonen, J., Lehto, V.-P., 2005. Mesoporous silicon microparticles for oral drug delivery: loading and release of five model drugs. J. Control. Release 108, 362–374.

Schmidt-Winkel, P., Lukens, W.W., Zhao, D., Yang, P., Chmelka, B.F., Stucky, G.D., 1999. Mesocellular siliceous foams with uniformly sized cells and windows. J. Am. Chem. Soc. 121, 254–255.

Slowing, I.I., Trewyn, B.G., Giri, S., Lin, V.S.-Y., 2007. Mesoporous silica nanoparticles for drug delivery and biosensing applications. Adv. Funct. Mater. 17, 1225–1236.

Song, S.W., Hidajat, K., Kawi, S., 2005. Functionalized SBA-15 materials as carriers for controlled drug delivery: influence of surface properties on matrix–drug interactions. Langmuir 21, 9568–9575.

Thomas, M.J.K., Slipper, I., Walunj, A., Jain, A., Favretto, M.E., Kallinteri, P., Douroumis, D., 2009. Inclusion of poorly soluble drugs in highly ordered mesoporous silica nanoparticles. Int. J. Pharm. 387, 272–277.

Vasconcelos, T., Sarmento, B., Costa, P., 2007. Solid dispersions as strategy to improve oral bioavailability of poor water soluble drugs. Drug Discov. Today 12, 1068–1075.

Wang, S., 2009. Ordered mesoporous materials for drug delivery. Microporous Mesoporous Mater. 117, 1–9.

Wong, S.M., Kellaway, I.W., Murdan, S., 2006. Enhancement of the dissolution rate and oral absorption of a poorly water soluble drug by formation of surfactant-containing microparticles. Int. J. Pharm. 317, 61–68.

Wu, Z., Jiang, Y., Kim, T., Lee, K., 2007. Effects of surface coating on the controlled release of vitamin B_1 from mesoporous silica tablets. J. Control. Release 119, 215–221.

Yang, P.P., Quan, Z.W., Lu, L.L., Huang, S.S., Lin, J., 2008. Luminescence functionalization of mesoporous silica with different morphologies and applications as drug delivery systems. Biomaterials 29, 692–702.

Yu, H., Zhai, Q.Z., 2009. Mesoporous SBA-15 molecular sieve as a carrier for controlled release of nimodipine. Microporous Mesoporous Mater. 123, 298–305.

Zhang, F., Aaltonen, J., Tian, F., Saville, D.J., Rades, T., 2009. Influence of particle size and preparation methods on the physical and chemical stability of amorphous simvastatin. Eur. J. Pharm. Biopharm. 71, 64–70.

Zhao, D.Y., Feng, J.L., Huo, Q.S., Melosh, N., Fredrickson, G.H., Chmelka, B.F., Stucky, G.D., 1998. Triblock copolymer syntheses of mesoporous silica with periodic 50 to 300 angstrom pores. Science 279, 548–552.